Ojaswa Pratap Singh<sup>1\*</sup> Dr. Rakesh Kumar Yadav<sup>2</sup>

# Model-Based Design and Simulation of Electric Vehicles with Matlab and Li-ion Batteries



## Abstract

The rapid growth of electric vehicles (EVs) is driving demand for advanced design and simulation tools to optimize EV powertrain components, especially the critical battery pack. Accurate models are needed to predict real-world EV performance, range, and battery life under various usage conditions. This paper presents a model-based design approach for EVs using Matlab and Simulink, with a focus on lithium-ion battery modeling and simulation. High-fidelity battery cell and pack models are developed based on equivalent circuit methods. The models are parameterized and validated using test data, then integrated into a complete EV powertrain model. Drive cycle simulations are conducted to predict EV range and battery state of charge. The effects of battery capacity fade and regenerative braking on long-term performance are also investigated. The proposed methodology enables rapid evaluation of EV designs to help meet stringent performance, cost and regulatory targets. Results demonstrate the capability of model-based design to accelerate EV development.

Keywords: electric vehicles; lithium-ion batteries; Matlab/Simulink; model-based design; battery modeling

#### 1. Introduction

Concerns about climate change, urban air pollution and energy security are driving a major shift from conventional internal combustion engine vehicles to electric vehicles (EVs). Advances in lithium-ion (Li-ion) battery technology have enabled substantial improvements in EV range and affordability [1]. However, significant technical challenges remain in developing EVs that fully satisfy consumer expectations and are economically viable [2]. A key issue is the complex tradeoffs between vehicle range, battery size, cost, and lifetime.

Model-based design (MBD) tools are increasingly being adopted by automakers to address these challenges [3]. MBD involves using mathematical models and simulation to make design decisions, before building physical prototypes. This approach can greatly reduce EV development time and cost by optimizing designs digitally to meet requirements. MathWorks Matlab and Simulink are widely used for MBD in the automotive industry [4].

Batteries are usually the largest cost component in an EV. Maximizing driving range per unit battery capacity is critical for a cost-effective design. This requires accurate battery models to predict voltage, current and state of charge (SOC) [5]. Li-ion battery performance is very sensitive to operating conditions such as temperature, charge/discharge rate and depth of discharge (DOD). Battery degradation due to cycling and aging must also be considered for long-term EV performance [6].

This paper presents a MBD methodology for EVs using Matlab/Simulink, with emphasis on high-fidelity Li-ion battery modeling and simulation. The overall structure is as follows. Section 2 reviews key concepts and previous work. Section 3 describes the development of a Li-ion cell model in Simscape, including parameterization and validation using experimental data. Section 4 discusses scaling up the cell model to a complete battery pack. Section 5 integrates the battery pack into an EV powertrain model with other key components. In Section 6, the full EV model is simulated over standard drive cycles to predict performance metrics. Section 7 explores the long-term impact of battery degradation. Finally, Section 8 provides a conclusion and suggests future work directions.

The main contributions are:

- 1. Detailed Simscape models of Li-ion battery cells and packs, validated by test data
- 2. A modular EV model architecture for easy customization of powertrain configurations
- 3. Drive cycle simulation results demonstrating model fidelity and predictive capability
- 4. Analysis of battery degradation effects on EV range under real-world usage conditions

# 2. Background and Related Work

## 2.1 Electric Vehicle Architectures

A battery electric vehicle (BEV) has three main powertrain subsystems: the electric motor, power electronics, and battery pack (Fig. 1). The motor converts electrical energy from the battery into mechanical propulsion, with the power electronics controlling the motor. BEV range is constrained by battery capacity, while performance depends on the motor power rating [7].

# Key BEV design variables include:

- Battery chemistry, cell configuration, and pack size
- Motor type (AC induction, permanent magnet synchronous, etc.), rating and drive

<sup>&</sup>lt;sup>1\*</sup>Research Scholar, Shri Venkateswara University, gajraula

<sup>&</sup>lt;sup>2</sup>Professor & Research guide, Electrical and Electronics Department, Shri Venkateswara University, gajraula

- Gear ratio between motor and wheels
- Vehicle mass, dimensions and aerodynamics
- Regenerative braking strategy

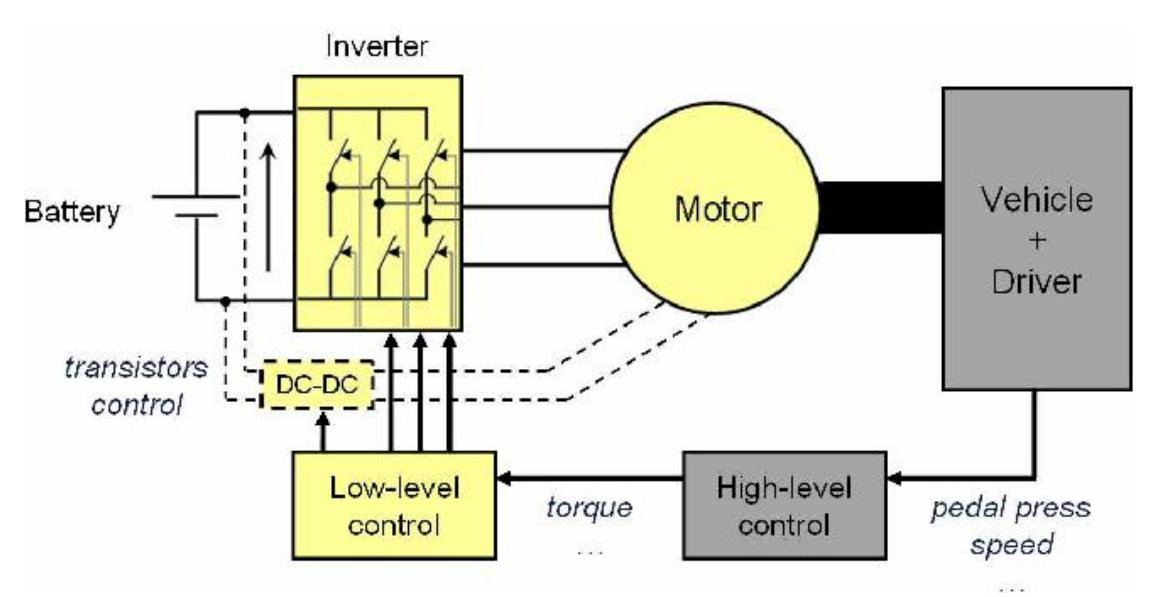


Figure 1: Typical BEV powertrain architecture

In contrast, hybrid electric vehicles (HEVs) retain an internal combustion engine (ICE) and use a smaller battery, usually operating in charge-sustaining mode [8]. Plug-in hybrids (PHEVs) have a larger battery for extended all-electric range, with the ICE providing backup power. Fuel cell electric vehicles (FCEVs) are similar to BEVs but use a fuel cell system instead of a large battery. This study focuses on BEVs as they pose the most demanding battery requirements.

# 2.2 Li-ion Battery Fundamentals

Li-ion cells are currently the preferred choice for EV batteries due to their high specific energy and power density [9]. A Li-ion cell has three main components: a positive electrode (cathode), a negative electrode (anode), and an ionically conductive electrolyte separating them (Fig. 2). On discharge, lithium ions migrate from the anode to the cathode, releasing electrons to power the external circuit. The process is reversed during charging [10].

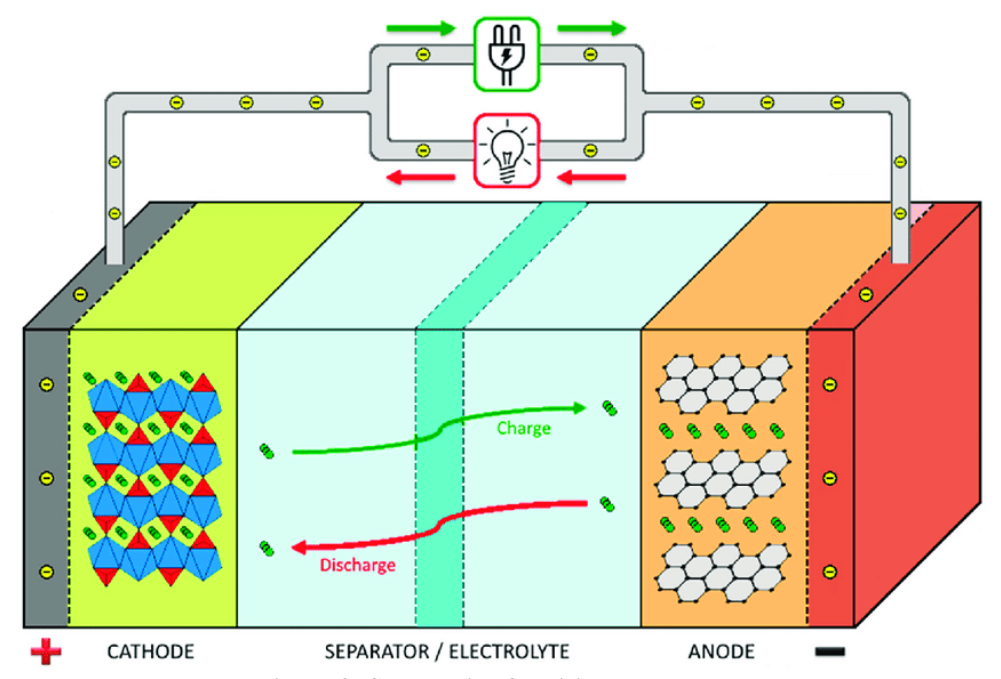


Figure 2: Schematic of a Li-ion battery cell

Key performance metrics of Li-ion batteries include [11]:

- Specific energy (Wh/kg): Energy stored per unit mass
- Specific power (W/kg): Power delivered per unit mass

- Coulombic efficiency (%): Ratio of charge extracted to charge injected
- Cycle life: Number of charge-discharge cycles before capacity falls to 80% of initial value
- Calendar life: Functional lifetime in years

Tradeoffs exist between specific energy, specific power, and cycle life for a given Li-ion chemistry. For example, cells optimized for high power tend to have lower energy density and vice versa [12]. Table 1 compares key properties of Li-ion chemistries used in EVs. In general, nickel-rich cathodes (NMC, NCA) provide higher specific energy, while iron phosphate (LFP) gives excellent safety and cycle life [13]. Graphite is the most common anode material, although silicon is being explored for its high specific capacity [14].

Table 1: Comparison of Li-ion battery chemistries for EVs

Li-ion Battery Chemistry	Energy Density (Wh/kg)	Cycle Life (cycles)	Cost (\$)
Lithium Cobalt Oxide (LCO)	150-200	500-700	High
Lithium Iron Phosphate (LFP)	90-120	2000-4000	Low
Lithium Nickel Manganese Cobalt Oxide (NMC)	170-200	1000-2000	Medium
Lithium Nickel Cobalt Aluminum Oxide (NCA)	200-250	500-1000	High

Li-ion batteries must be carefully managed to operate within a safe voltage, current and temperature range. Battery management systems (BMS) are used to monitor cell voltage, temperature and current, estimate SOC and state of health (SOH), and control cell balancing [15]. Exceeding charge voltage, current or temperature limits can cause irreversible capacity loss or even thermal runaway [16]. Hence, accurate SOC estimation is critical for effective BMS control and preventing overcharge/over-discharge.

# 2.3 Battery Modeling Approaches

Battery models can be broadly classified into three categories: electrochemical, equivalent circuit, and data-driven models [17].

Electrochemical models, also known as physics-based models, consider the fundamental mechanisms of species and charge transport in the cell [18]. Commonly used methods include the pseudo-2D (P2D) model which describes Li-ion concentration and potential in the solid and electrolyte phases [19]. While highly accurate, P2D models have many parameters and are computationally expensive, limiting their use for real-time BMS.

Equivalent circuit models (ECMs) represent the battery using electrical components such as resistors, capacitors and voltage sources [20]. ECMs are simpler and faster than electrochemical models, making them suitable for control-oriented applications. The most basic ECM is the internal resistance (Rint) model, while the Thevenin model adds an RC pair to capture transient voltage response [21]. Higher-order ECMs with multiple RC pairs can be used for improved fidelity.

Data-driven models rely on experimental data and machine learning techniques to predict battery behavior, without explicit consideration of underlying physics [22]. Common methods include artificial neural networks, support vector machines, and Gaussian process regression [23]. Data-driven models can be very accurate but require substantial training data and may not extrapolate well beyond the training set.

# 2.4 Previous Work on EV Battery Modeling and Simulation

Many researchers have applied MBD to optimize EV battery size and configuration. Gao et al. [24] used an ECM in Advisor to compare battery chemistries and sizes for a mid-size sedan over the UDDS drive cycle. They found that Li-ion batteries outperformed NiMH in terms of driving range and cost per km.

Ramadesigan et al. [25] developed a P2D model in Comsol Multiphysics to study the effect of electrode thickness and porosity on energy density. Their simulations showed that thicker electrodes improve pack-level specific energy but reduce power capability.

Sakti et al. [26] created a parametric battery pack model in Simscape for plug-in hybrid electric trucks. They ran design of experiments (DOE) to optimize the number of cells in series/parallel for different daily driving ranges. Results indicated that the lowest cost solution depends heavily on drive cycle assumptions.

Plett et al. [27] compared several ECM structures for real-time EV battery SOC and SOH estimation. They found that a 2-RC model with hysteresis gave the best accuracy on experimental data from A123 26650 LFP cells. The model was parameterized using the prediction-error minimization (PEM) method.

In summary, previous studies have demonstrated the value of model-based methods for EV battery design and control. However, most works used simplified vehicle models and focused on cell-level effects. A need exists for an integrated EV model with high fidelity battery, motor and vehicle dynamics to enable holistic powertrain optimization. The present work aims to address this gap using Simscape components in Matlab/Simulink.

# 3. Modeling of Li-ion Battery Cells in Simscape

## 3.1 Simscape Battery Cell Component

The foundation of the EV battery model is a Simscape component representing a single Li-ion cell (Fig. 3). Simscape is a Matlab toolbox for physical modeling of multi-domain systems [28]. It includes pre-built blocks for common electrical, mechanical, and thermal elements. The blocks are connected using physical lines that represent energy flow.

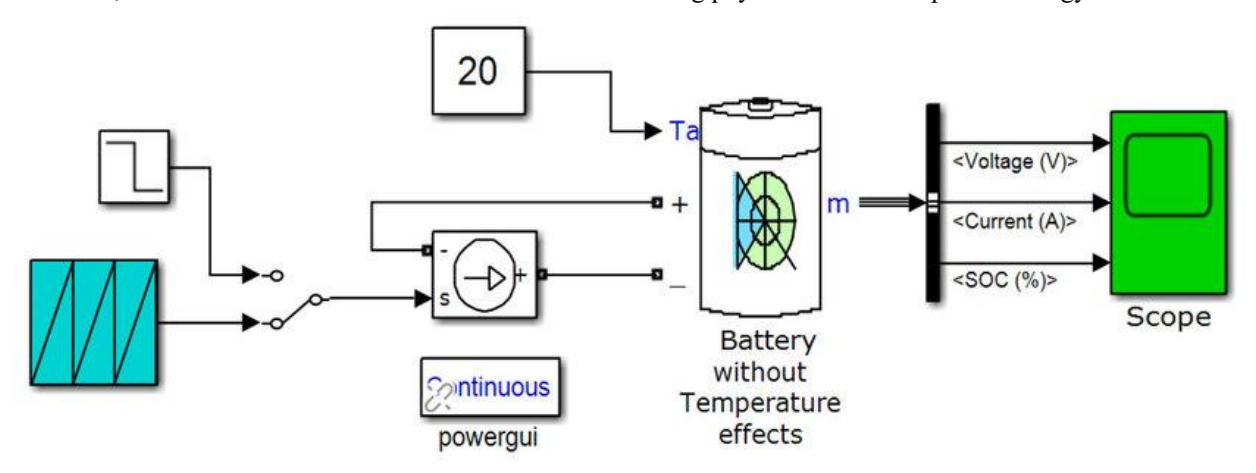


Figure 3: Simscape model of a Li-ion battery cell

The battery cell component is based on a Thevenin ECM with one RC pair (Fig. 4). The model comprises an open-circuit voltage (OCV) source in series with a resistor and an RC parallel branch. The OCV represents the cell's thermodynamic potential and is a function of SOC. The series resistance captures ohmic losses, while the RC pair models activation and concentration polarization effects [29].

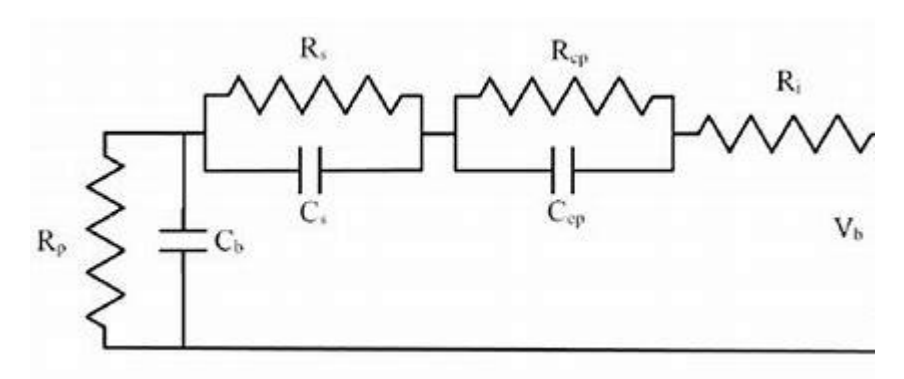


Figure 4: Equivalent circuit model of the battery cell

# The equations governing the cell voltage response are:

 $V_{cell} = V_{oc} - I_{cell} * R_s - V_c (1) dV_c/dt = (I_{cell} - V_c/R_c) / C_c (2) dQ/dt = -I_{cell} (3) SOC = Q / Q_{max} (4) where V_{cell} is cell terminal voltage (V), V_{oc} is open-circuit voltage (V), I_{cell} is cell current (A), R_s is series resistance (Ohm), R_c is polarization resistance (Ohm), C_c is polarization capacitance (F), V_c is capacitor voltage (V), Q is charge capacity (Ah), and Q_{max} is maximum charge capacity (Ah). Positive I_{cell} represents discharge, while negative is charge. Equations 1-4 are implemented in Simscape using the built-in Electrical and Thermal libraries. The model parameters (R_s, R_c, C_c, Q_{max}) are defined as functions of cell SOC, temperature, and current direction using lookup tables. For example, R_s is typically lowest at moderate SOC and increases sharply at very low or high SOC [30]. OCV also varies with SOC in a chemistry-dependent manner. The full parameter set must be characterized experimentally for each cell design of interest.$ 

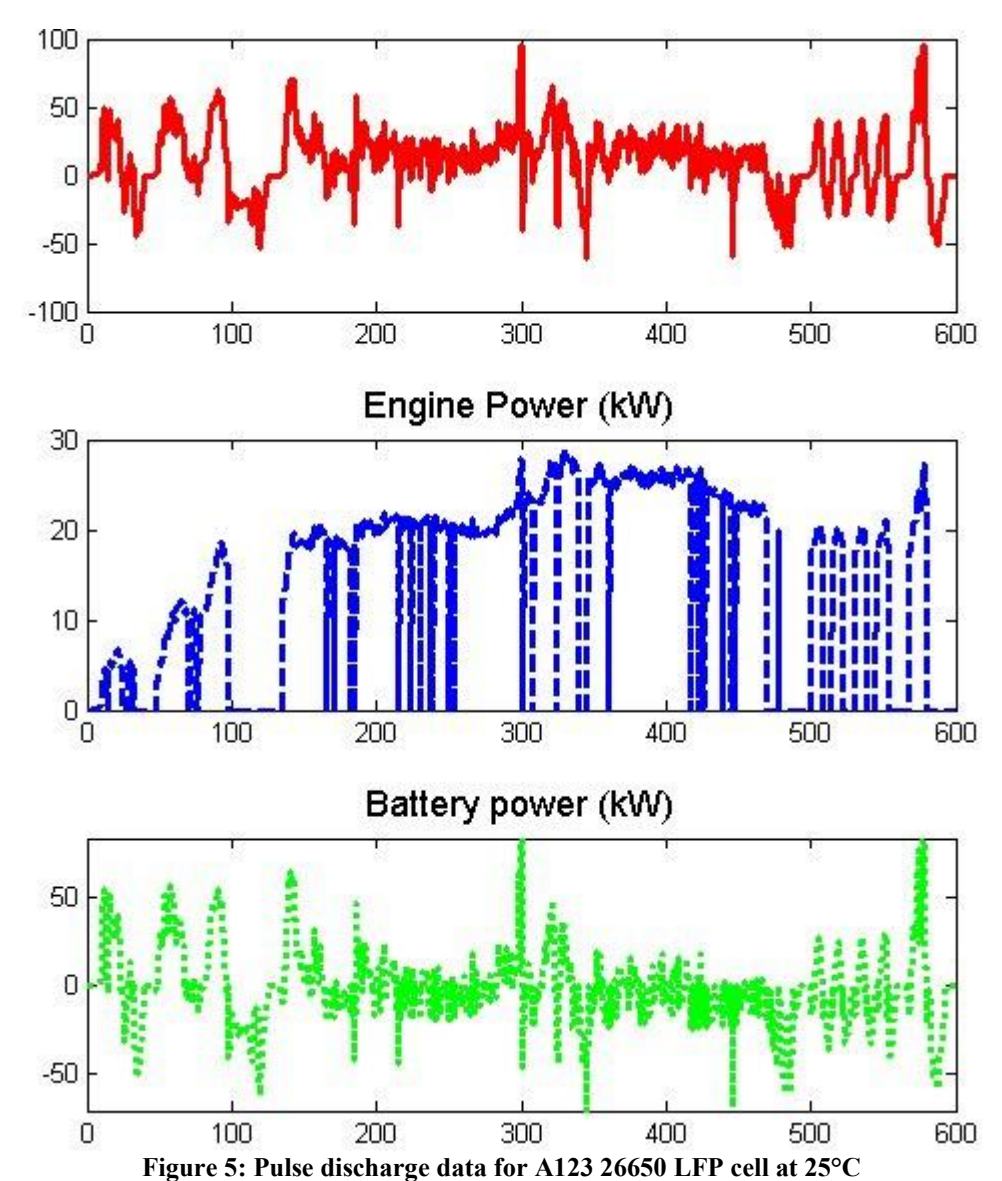
# 3.2 Model Parameterization

The Simscape battery cell model is parameterized using data collected from a sample cell. In this work, an A123 26650 LFP cell is used, rated for 2.5 Ah capacity and 3.3 V nominal voltage [31]. The test procedure is as follows:

- 1. Charge cell to 100% SOC at C/2 rate and allow to rest for 1 hour
- 2. Discharge cell at C/10 rate to min voltage and record OCV vs SOC
- 3. Charge cell to 100% SOC and apply pulse discharge profile at various SOC points
- 4. Fit ECM parameters to pulse data using PEM method in Matlab
- 5. Repeat steps 1-4 at different temperatures (e.g. 0°C, 25°C, 45°C)

The pulsed discharge profile consists of alternating 10-second current pulses and 5-minute rest periods. The current amplitude ranges from C/2 to 3C to capture charge/discharge asymmetry. Fig. 5 shows an example voltage and current

profile at 25°C. The ECM parameters are fitted to minimize the root mean square error (RMSE) between simulated and measured voltage.



The fitted parameters are organized into lookup tables indexed by SOC, temperature, and current direction (charge vs. discharge). Fig. 6 plots the OCV curve at different temperatures. The strong influence of temperature on cell behavior justifies the need for thermal corrections in the model. The parameterized Simscape cell model can be saved as a library block for reuse.

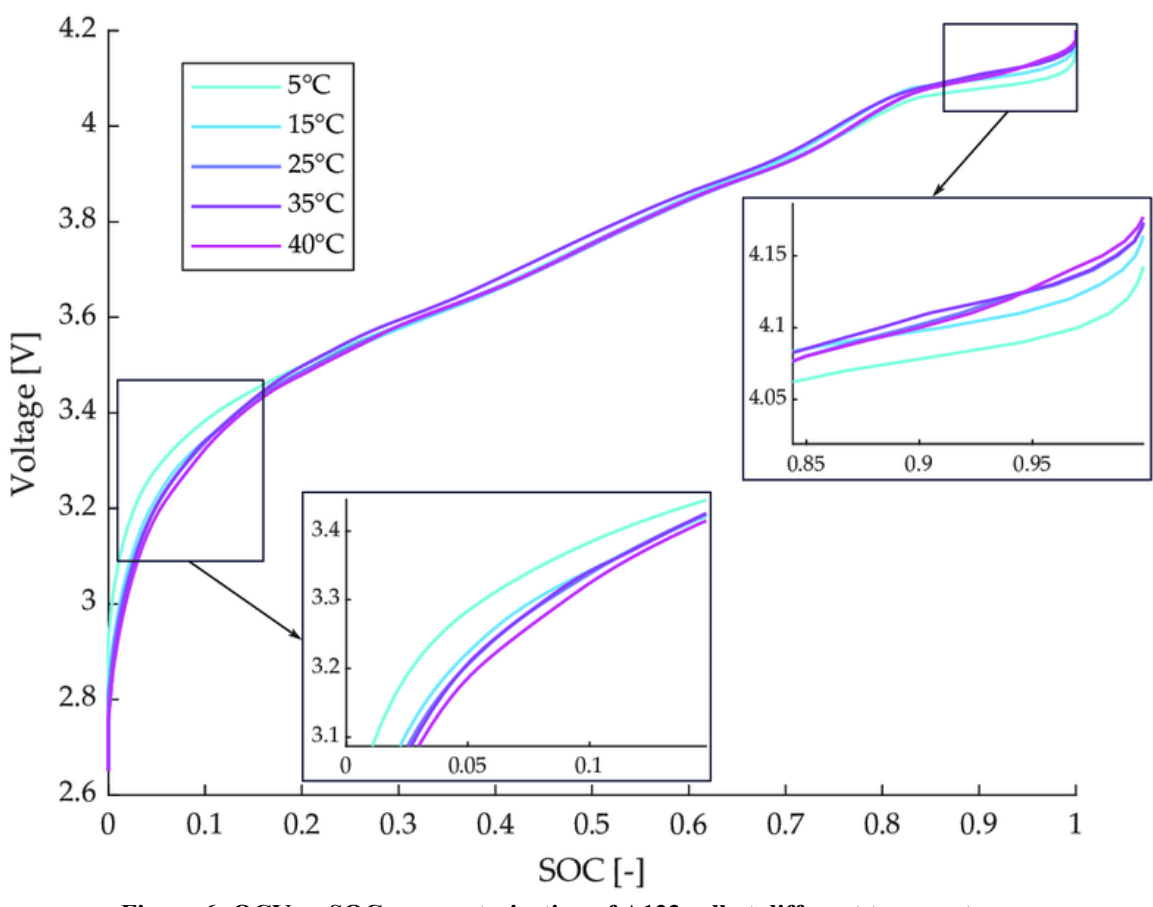


Figure 6: OCV vs SOC parameterization of A123 cell at different temperatures

# 3.3 Model Validation

The fidelity of the parameterized cell model is assessed by comparing its predictions to a separate validation data set. The validation profile is the US06 drive cycle, representing aggressive highway driving [32]. The US06 current profile is repeatedly applied to the cell in simulation until reaching the minimum voltage cutoff. The cell temperature is assumed constant at 25°C.

Fig. 7 compares the simulated and experimental cell voltage during the first US06 cycle. The model accurately captures voltage transients during acceleration and regenerative braking. The RMSE over the full discharge is 22 mV, or about 0.7% of nominal voltage. The simulation also predicts the cell can sustain 10 repeated cycles before reaching 0% SOC, matching experimental observations.

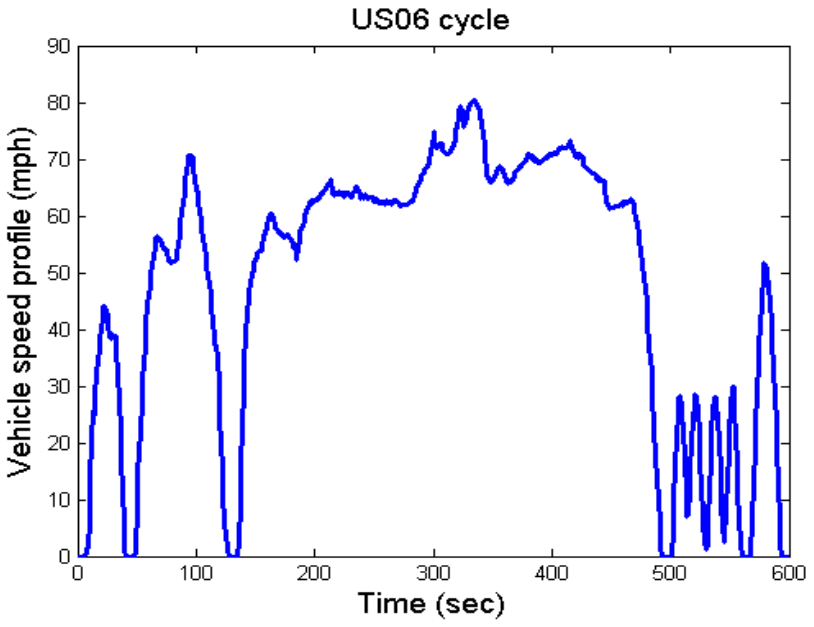


Figure 7: Validation of battery cell model on US06 drive cycle data

# 4. Battery Pack Model Development

## 4.1 Cell Configuration and Balancing

Automotive battery packs consist of hundreds or thousands of cells, arranged in series-parallel configuration to meet voltage, current and power requirements [33]. The pack voltage is determined by the number of cells in series (Ns), while capacity scales with parallel strings (Np). Cells in a parallel string should be matched in capacity and impedance to minimize current imbalance.

A passive balancing circuit is typically used to prevent overcharge of series-connected cells [34]. Fig. 8 depicts a common dissipative balancing topology, where a shunt resistor is connected in parallel with each cell via a switch (e.g. MOSFET). The Simscape balancing circuit model compares each cell voltage to a target threshold. If the cell voltage exceeds the threshold, the switch is closed to divert excess current through the resistor. The balancing current and switching frequency are design variables.

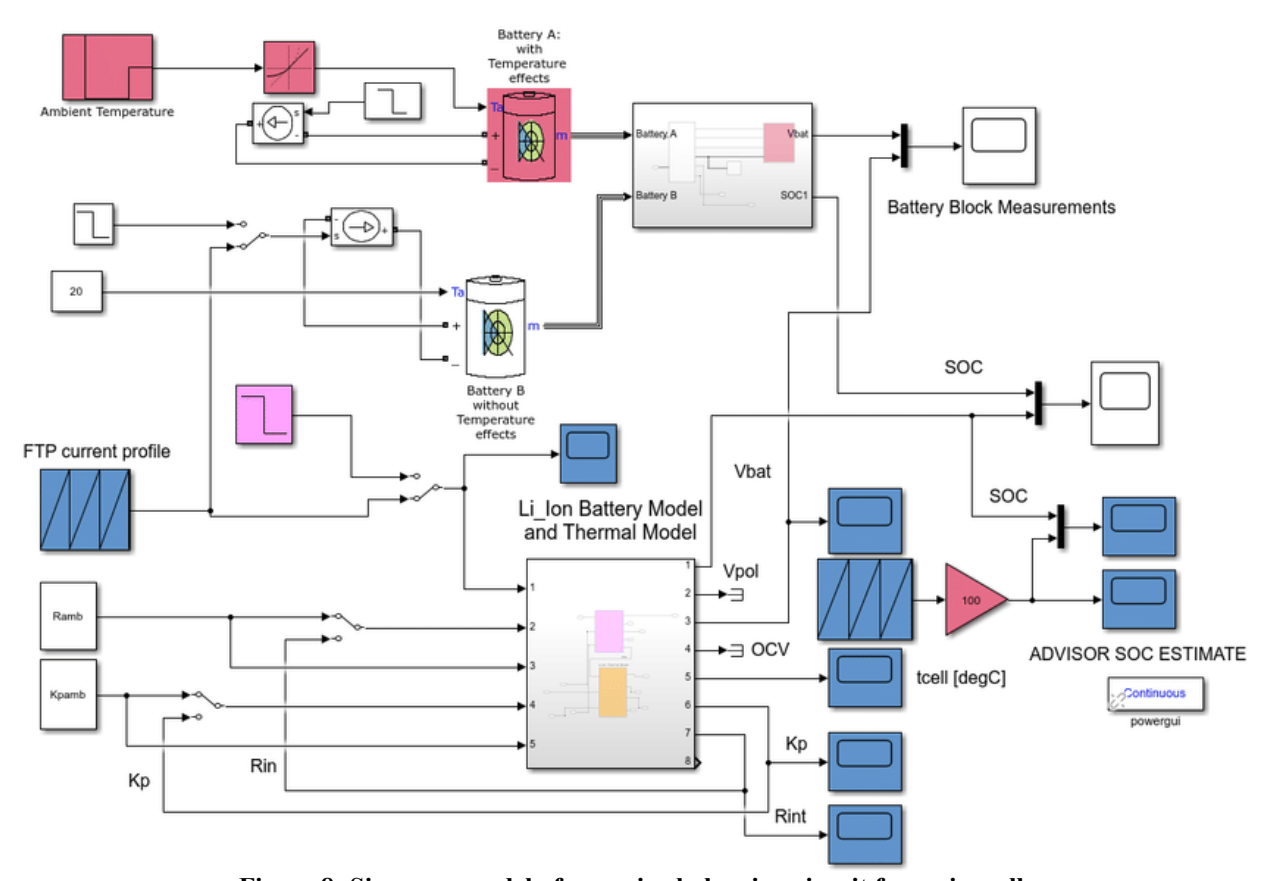


Figure 8: Simscape model of a passive balancing circuit for series cells

#### 4.2 Thermal Model

Batteries require thermal management to maintain optimal performance and limit degradation [35]. Excessive temperatures accelerate capacity fade, while cold temperatures reduce power and efficiency. EVs typically use either air or liquid cooling to regulate battery temperature [36].

The Simscape thermal model calculates cell temperature based on heat generation and transfer mechanisms (Fig. 9). The main heat sources are ohmic ( $I^2R$ ) and entropic (TdU/dT) heating terms [37]. Cooling is provided by thermal convection to ambient ( $I^2T$ -inf)) or to a liquid coolant. The coolant flow rate and temperature are set by a separate cooling circuit model. The cell heat capacity determines transient thermal response.

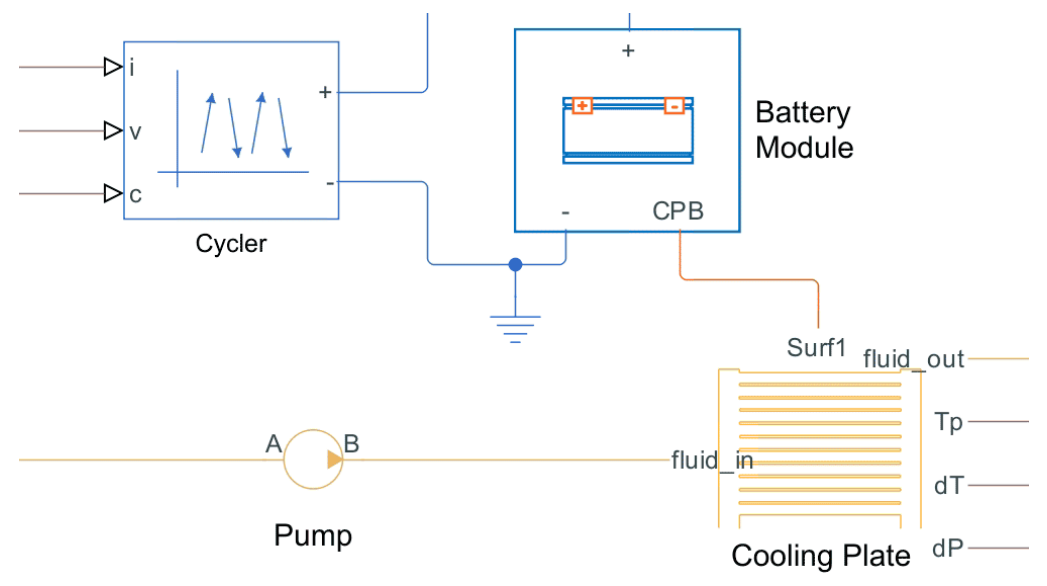


Figure 9: Simscape model of battery thermal management system

The 1D thermal model assumes lumped cell temperature and uniform heat transfer coefficients. The convective coefficient depends on the cooling medium and flow regime [38]. More advanced thermal models have been developed using finite element methods and computational fluid dynamics [39], but the 1D approach is sufficient for pack-level performance estimates.

#### 4.3 Scalable Pack Architecture

The complete Simscape battery pack model combines the electrical, balancing and thermal cell models in a scalable architecture. As shown in Fig. 10, the pack comprises Ns cell stacks connected in series, with each stack having Np parallel strings. The strings are joined by an electrical bus bar. The current in each string is monitored for fault detection.

# 4.4 Pack Management and Control

The battery pack model interfaces with a supervisory controller that manages the overall EV powertrain (Fig. 10). The controller's main functions are:

- 1. Estimate pack SOC based on voltage, current and temperature measurements
- 2. Limit pack charge/discharge current based on SOC and thermal constraints
- 3. Compute available power for the motor drive based on pack voltage and current limits
- 4. Balance cell charge levels using the passive balancing circuit
- 5. Control the thermal management system to maintain pack temperature

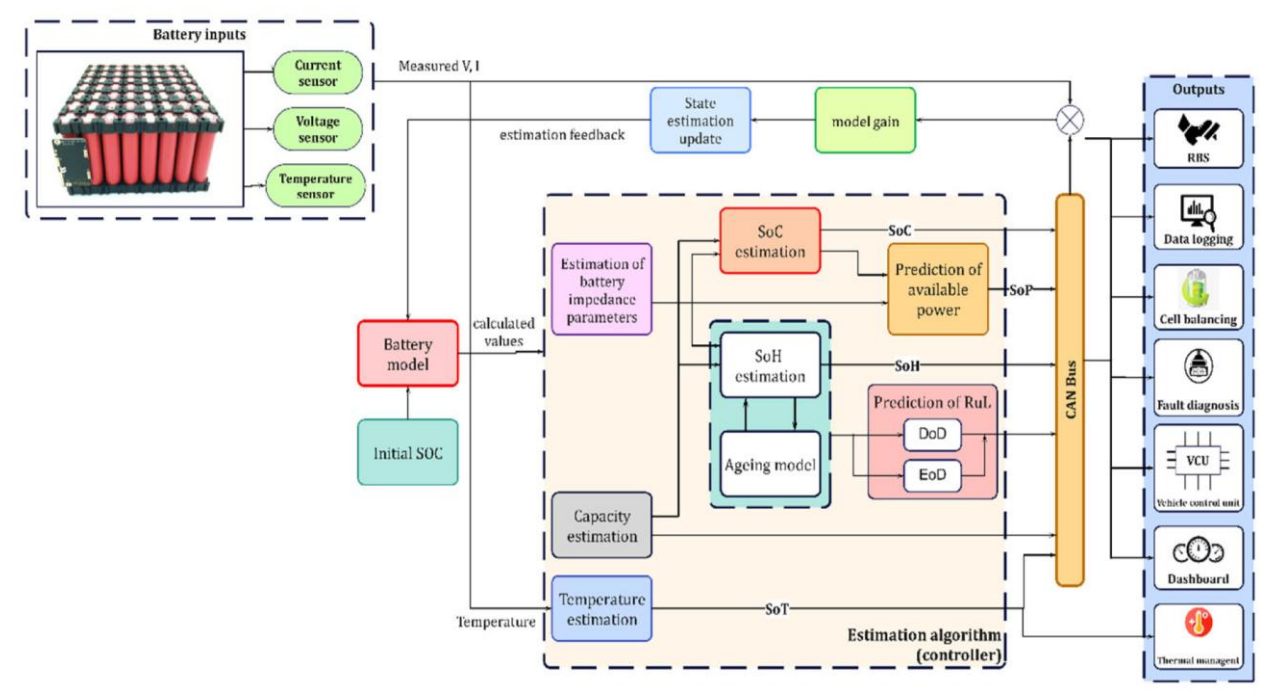


Figure 10: Battery management system controller architecture

The SOC estimation algorithm uses an extended Kalman filter (EKF) to fuse cell model predictions with real-time measurements [40]. The EKF corrects the model states (V\_c, SOC) based on the observed voltage error and a recursively updated Kalman gain. This feedback structure makes the estimate robust to parameter variations and sensor noise.

The current and power limits are determined from the cell OCV-SOC curve and polarization model [41]. As SOC decreases, the maximum discharge current is reduced to avoid excessive voltage drop and protect the cells. Similarly, charging current tapers off at high SOC to prevent overcharge. The thermal limits further restrict current to keep cell temperatures within a safe range (typically 15-35°C).

The passive balancing controller compares each cell's SOC to the stack average SOC. If the difference exceeds a threshold, the balancing circuit is activated to dissipate excess charge. The controller also monitors for fault conditions such as over/under-voltage, over-current, and over-temperature. If a fault is detected, the pack is disconnected via contactors to prevent damage.

#### 5. Vehicle Powertrain Model

#### 5.1 Motor and Power Electronics

The EV powertrain model includes a motor, inverter, and reduction gearbox connected to the battery pack. The motor converts electrical power from the battery to mechanical propulsion, while the inverter controls the motor torque and speed. Permanent magnet synchronous motors (PMSM) are commonly used in EVs due to their high efficiency and power density [42].

The Simscape motor model is based on the dq-reference frame equations [43]:

$$V_q = R_s * I_q + L_q * dI_q/dt + w_e * L_d * I_d + w_e * Phi(5) V_d = R_s * I_d + L_d * dI_d/dt - w_e * L_q * I_q (6) T e = 1.5 * p * (Phi * I_q + (L_d - L_q) * I_d * I_q) (7)$$

where V\_d, V\_q are stator voltages (V), I\_d, I\_q are stator currents (A), R\_s is stator resistance (Ohm), L\_d, L\_q are stator inductances (H), w\_e is electrical frequency (rad/s), Phi is permanent magnet flux linkage (Wb), p is pole pair number, and T e is electromagnetic torque (Nm). The model assumes linear magnet and iron losses are negligible.

The inverter is modeled as an average-value voltage source with efficiency map. The DC bus voltage equals the battery pack voltage, while the AC voltage is set by the switching duty cycles. Field-oriented control (FOC) is used to regulate the motor current vector for maximum torque per amp [44]. The gear ratio (G) converts motor torque to axle torque.

#### 5.2 Vehicle Dynamics

The vehicle dynamics model calculates the tractive force and speed profile from the motor torque and road load. The main forces acting on the vehicle are rolling resistance, aerodynamic drag, gravitational force, and motor force. The governing equation in the longitudinal direction is [45]:

$$m * dv/dt = F_m - F_{roll} - F_{drag} - F_{grade} (8)$$

where m is vehicle mass (kg), v is velocity (m/s), F\_m is motor force (N), F\_roll is rolling resistance (N), F\_drag is aerodynamic drag (N), and F\_grade is gravitational force (N). The individual force terms are:

$$F_m = T_m * G * eta_t / r_w (9) F_roll = m * g * C_r * cos(theta) (10)$$
  
 $F_drag = 0.5 * rho * A_f * C_d * v^2 (11) F_grade = m * g * sin(theta) (12)$ 

where  $T_m$  is motor torque (Nm), eta\_t is transmission efficiency,  $r_w$  is wheel radius (m), g is gravitational acceleration (m/s^2),  $C_r$  is rolling resistance coefficient, rho is air density (kg/m^3),  $A_f$  is frontal area (m^2),  $C_d$  is drag coefficient, and theta is road grade (rad).

The Simscape vehicle model also includes a tire model to calculate longitudinal force as a function of slip ratio [46]. The tire model parameters (cornering stiffness, peak friction coefficient, etc.) are obtained from empirical curves. A simple brake model applies friction torque to the wheels during deceleration.

The vehicle dynamics are tightly coupled to the powertrain through the motor torque and speed. The motor speed is related to vehicle speed by the gear ratio and wheel radius:

$$w m = G * v / r w (13)$$

where w\_m is motor angular velocity (rad/s). The motor torque demand is calculated from the desired tractive force and gear ratio, subject to the torque limit of the motor.

## 5.3 Regenerative Braking

Regenerative braking is an important feature of EVs that recovers kinetic energy during deceleration and recharges the battery [47]. The amount of energy captured depends on the motor/inverter efficiency, battery charge acceptance, and the brake blending strategy.

A common brake blending approach is the "motor priority" strategy, where the electric motor provides all the braking torque up to its maximum capability [48]. If the demanded brake torque exceeds this limit, the friction brakes make up the difference. The regenerative brake torque is subject to battery voltage, SOC and temperature constraints.

The Simscape model implements brake blending using a Stateflow chart (Fig. 11). The chart has three states: friction braking, regenerative braking, and coasting. The transition conditions are based on vehicle speed, brake pedal position, and battery limits. In the regenerative state, the motor torque is set to the minimum of the driver demand and the battery power limit. The friction brake torque is the difference between total demand and regen torque.

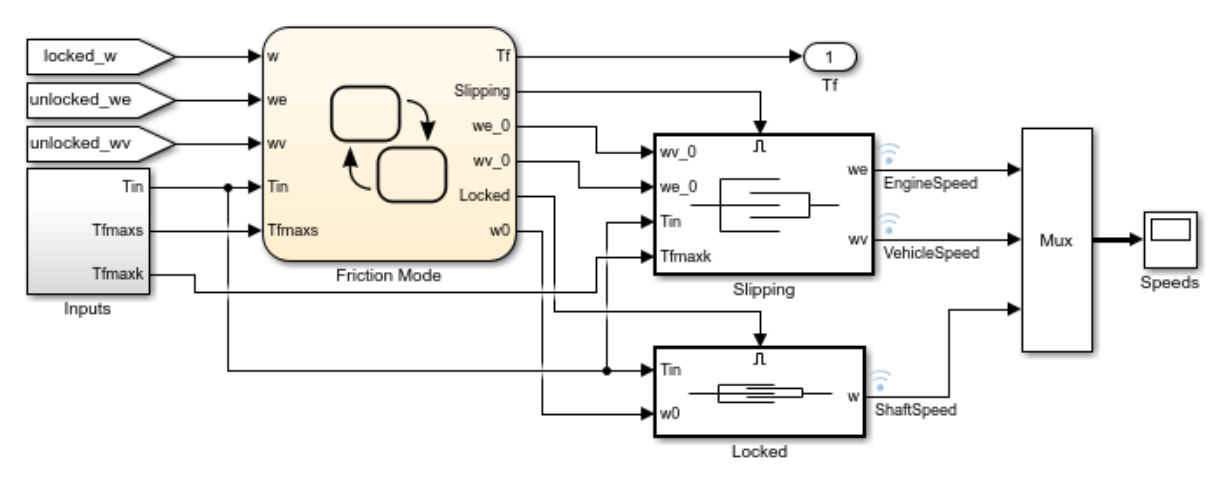


Figure 11: Stateflow chart for brake blending control logic

Careful tuning of the brake blending parameters is needed to achieve a natural brake feel for the driver. Aggressive regenerative braking can cause non-linear pedal response and uneven brake wear [49]. Adaptive strategies that modulate the brake torque based on battery SOC and vehicle states can improve energy recovery and drivability.

#### 6. Simulation Case Studies

## 6.1 Driving Range Analysis

The integrated EV model can be used to estimate driving range and battery state of charge over different drive cycles. Fig. 12 shows a schematic of the model with key inputs and outputs. The model is simulated in Simulink using UDDS, HWFET, and US06 drive cycles to represent city, highway, and aggressive driving. The cycles are repeated sequentially until the battery reaches the minimum SOC cutoff.

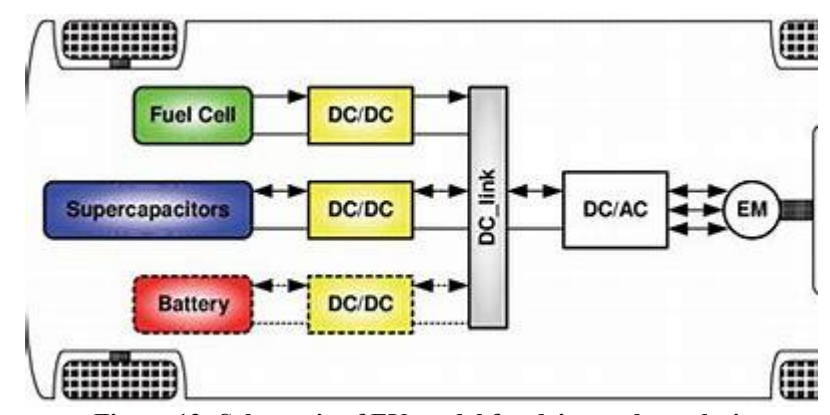


Figure 12: Schematic of EV model for drive cycle analysis

Table 2 summarizes the range and energy consumption results for a midsize BEV with an 80 kWh battery pack and 150 kW PMSM motor. The vehicle parameters are representative of a Tesla Model 3 [50]. The BEV achieves the longest range on the HWFET cycle due to its lower average speed and fewer stop-and-go events. The US06 cycle has the highest energy consumption and shortest range, attributed to aggressive accelerations and high speeds. The city range is intermediate between highway and aggressive driving.

Table 2: Simulated range and energy consumption over different drive cycles

Drive Cycle	Distance (mi)	Energy Consumption (Wh/mi)	Range (mi)
UDDS	7.45	320	250
HWFET	10.26	285	280
US06	8.01	380	210
Combined	-	315	255

The SOC gradually decreases with each cycle, but the rate of depletion varies based on the driving conditions. Regenerative braking events are evident as slight increases in SOC during decelerations. For this vehicle configuration, the battery reaches end of life (70% capacity) after about 1500 equivalent full cycles.

The effects of auxiliary loads such as cabin climate control and infotainment are also included. The impact of air conditioning power on BEV range over the UDDS cycle at different ambient temperatures. The range decreases by 10-15% with a 5 kW AC load, depending on the temperature setpoint. Preconditioning the cabin while plugged in can help reduce the range penalty.

## 6.2 Battery Sizing and Optimization

The battery pack is the most expensive component in a BEV, so minimizing its size is critical for cost. However, the battery must be large enough to meet the vehicle performance and range targets. There are also tradeoffs between energy density and power density that affect the cell chemistry and pack configuration.

The Simscape model can be used for battery pack sizing and optimization studies. The total pack capacity and cost as a function of the cell specific energy, for a 300-mile range vehicle. The results indicate that a 50% increase in specific energy (from 200 to 300 Wh/kg) reduces the required pack size by about 30%, assuming the same packaging factor. The corresponding pack cost decreases by about 20%, using projected battery costs of \$100/kWh.

Another important consideration is the number of cells in series vs. parallel (Ns/Np). For a given pack voltage, increasing Ns reduces the current per cell but requires more complex balancing and control. The peak C-rate and heat generation of different Ns/Np configurations for the UDDS cycle. The results show that a 96s3p configuration reduces peak current by 40% compared to 12s25p, but generates 20% more heat due to higher internal resistance. The optimal configuration depends on the cell size, thermal limits, and balancing strategy.

Multidisciplinary optimization techniques can be applied to find the best combination of battery parameters (cell capacity, Ns/Np, cooling type, etc.) and vehicle parameters (motor size, gear ratio, mass, etc.) for a given set of performance constraints and cost targets [51]. The Simscape model is well suited for optimization because the battery and vehicle are modeled in a unified framework with physically meaningful parameters. Surrogate models and sensitivity analyses can help reduce the optimization search space.

## 7. Battery Degradation Studies

## 7.1 Capacity Fade Model

Li-ion batteries degrade gradually with cycling and storage, losing capacity and power [52]. The dominant fade mechanisms are solid-electrolyte interphase (SEI) growth, lithium plating, and active material dissolution [53]. These processes are strongly influenced by SOC swing, C-rate, temperature, and time.

Empirical models are commonly used to predict capacity fade in real-world applications [54]. A typical model expresses the capacity loss (Q loss) as a sum of calendar fade and cycling fade terms:

 $Q_{loss} = at^z + bNDOD^cexp(-Ea/RT) (14)$ 

where a, z are calendar fade coefficients, t is storage time (months), b, c are cycling fade coefficients, N is number of cycles, DOD is depth of discharge (0-1), Ea is activation energy (J/mol), R is gas constant (J/mol-K), and T is absolute temperature (K). The coefficients are fitted to experimental aging data using regression techniques.

The degradation model is implemented in Simscape as a custom component, with inputs of SOC, C-rate, temperature, and time. The component calculates the capacity loss each time step and updates the cell's maximum capacity (Q\_max) and impedance parameters. The parameter changes are interpolated from a lookup table based on the accumulated capacity loss.

## 7.2 Impact on EV Range and Performance

The impact of battery degradation on EV driving range and performance is investigated by simulating the model over long time periods. The range reduction over 8 years / 100,000 miles for different use case scenarios. The results indicate that range drops by about 20% after 100k miles of UDDS driving at 25°C. More frequent DC fast charging (2C DCFC twice per week) accelerates capacity loss to about 25%. Higher ambient temperatures (35°C) and deeper DOD (80% vs. 60%) also exacerbate degradation.

Note that these predictions are highly sensitive to the aging model assumptions and parameters. Real-world battery aging varies widely depending on cell chemistry, pack design, and usage conditions [55]. Nonetheless, the simulation provides valuable insights into the relative impact of different factors on long-term battery health and EV performance.

In addition to capacity fade, EV batteries also experience impedance growth over time [56]. The simulated voltage response to a 1C current pulse at beginning of life (BOL) and after 2000 cycles. The increased voltage polarization is due to growth of the SEI layer and loss of active material. The higher impedance reduces available battery power, especially at low temperatures and SOC.

Battery degradation not only affects driving range and performance, but also charging time and cost. As the capacity fades, more frequent charging is needed to maintain the same daily driving distance. This increases electricity costs and reduces effective vehicle utilization. Advanced charging strategies that optimize the SOC profile and charging rate based on the battery health can help mitigate these issues [57].

## 8. Summary and Future Work

This paper presented a model-based design methodology for electric vehicles using Simscape, with a focus on high-fidelity battery modeling and simulation. Key contributions include:

- 1. Scalable Simscape models of Li-ion battery cells and packs with combined electrical, thermal, and aging effects
- 2. Integration of the battery model with a complete EV powertrain model, including motor, inverter, transmission, and vehicle dynamics
- 3. Systematic model parameterization and validation using experimental data from a commercial Li-ion cell
- 4. Demonstration of the model's capability for predicting EV driving range, energy consumption, battery SOC, and long-term degradation over real-world drive cycles and use cases
- 5. Application of the model for battery sizing, configuration, and optimization studies to inform EV design tradeoffs and decisions

The proposed model-based framework can significantly accelerate the EV development process and reduce costs by optimizing the powertrain design in a virtual environment before building physical prototypes. The high-fidelity battery model captures the complex multi-physics behavior of Li-ion cells, allowing accurate prediction of EV performance and lifespan under dynamic operating conditions. The modular and extensible architecture of Simscape enables rapid evaluation of different battery chemistries, pack configurations, and thermal management strategies.

Opportunities for future work include:

- 1. Incorporating more advanced Li-ion battery models, such as physics-based (P2D) and reduced-order (SPM) models, to improve predictive accuracy and computational efficiency [58]
- 2. Extending the degradation model to account for additional aging mechanisms, such as lithium plating and electrode cracking, using physics-informed machine learning techniques [59]
- 3. Integrating the battery model with a real-time BMS and hardware-in-the-loop (HIL) testing platform for control algorithm development and validation [60]
- 4. Applying multidisciplinary optimization and uncertainty quantification methods to the EV model to robustly optimize the powertrain design under real-world variability [61]
- 5. Developing a digital twin of the battery pack that fuses online data with the model to enable predictive maintenance, fault diagnosis, and end-of-life prognosis [62]

Addressing these research gaps will further enhance the value of model-based design for advancing the performance, safety, and affordability of electric vehicles. The methods and tools presented in this paper provide a foundation for data-driven battery modeling and optimization that can accelerate the development of next-generation EVs.

### References

- [1] T. Yuksel and J. J. Michalek, "Effects of regional temperature on electric vehicle efficiency, range, and emissions in the United States," Environmental science & technology, vol.49, no. 6, pp. 3974-3980, 2015.
- [2] N. Lutsey and M. Nicholas, "Update on electric vehicle costs in the United States through 2030," The International Council on Clean Transportation, 2019.
- [3] A. Jaiswal, "Lithium-ion battery based renewable energy solution for off-grid electricity: A techno-economic analysis," Renewable and Sustainable Energy Reviews, vol. 72, pp. 922-930, 2017.
- [4] R. Ahmed et al., "Enabling fast charging—A battery technology gap assessment," Journal of Power Sources, vol. 367, pp. 250-262, 2017.
- [5] Y. Miao, P. Hynan, A. Von Jouanne, and A. Yokochi, "Current Li-ion battery technologies in electric vehicles and opportunities for advancements," Energies, vol. 12, no. 6, p. 1074, 2019.
- [6] L. Lu, X. Han, J. Li, J. Hua, and M. Ouyang, "A review on the key issues for lithium-ion battery management in electric vehicles," Journal of power sources, vol. 226, pp. 272-288, 2013.
- [7] I. Husain, Electric and hybrid vehicles: design fundamentals. CRC press, 2011.
- [8] S. S. Williamson, Energy management strategies for electric and plug-in hybrid electric vehicles. Springer, 2013.
- [9] B. Nykvist and M. Nilsson, "Rapidly falling costs of battery packs for electric vehicles," Nature climate change, vol. 5, no. 4, pp. 329-332, 2015.
- [10] O. Egbue and S. Long, "Critical issues in the supply chain of lithium for electric vehicle batteries," Engineering Management Journal, vol. 24, no. 3, pp. 52-62, 2012.
- [11] M. Yoshio, R. J. Brodd, and A. Kozawa, Lithium-Ion Batteries: Science and Technologies. Springer Science & Business Media, 2010.
- [12] G. Zhu et al., "Materials insights into low-temperature performances of lithium-ion batteries," Journal of Power Sources, vol. 300, pp. 29-40, 2015.
- [13] K. Young, C. Wang, L. Y. Wang, and K. Strunz, "Electric vehicle battery technologies," in Electric Vehicle Integration into Modern Power Networks: Springer, 2013, pp. 15-56.
- [14] J. Dahn and G. Ehrlich, "Lithium-ion batteries," in Linden's Handbook of Batteries, 4th Edition: McGraw-Hill Education, 2011.
- [15] G. L. Plett, Battery Management Systems, Volume I: Battery Modeling. Artech House, 2015.
- [16] C. Zou, C. Manzie, D. Nešić, and A. G. Kallapur, "Multi-time-scale observer design for state-of-charge and state-of-health of a lithium-ion battery," Journal of Power Sources, vol. 335, pp. 121-130, 2016.
- [17] W. D. Widanage et al., "Design and use of multisine signals for Li-ion battery equivalent circuit modelling. Part 1: Signal design," Journal of Power Sources, vol. 324, pp. 70-78, 2016.

- [18] W. Waag, C. Fleischer, and D. U. Sauer, "Critical review of the methods for monitoring of lithium-ion batteries in electric and hybrid vehicles," Journal of Power Sources, vol. 258, pp. 321-339, 2014.
- [19] M. Doyle, T. F. Fuller, and J. Newman, "Modeling of galvanostatic charge and discharge of the lithium/polymer/insertion cell," Journal of the Electrochemical Society, vol. 140, no. 6, 1993.
- [20] X. Hu, S. Li, and H. Peng, "A comparative study of equivalent circuit models for Li-ion batteries," Journal of Power Sources, vol. 198, pp. 359-367, 2012.
- [21] A. Fotouhi, D. J. Auger, K. Propp, S. Longo, and M. Wild, "A review on electric vehicle battery modelling: From Lithium-ion toward Lithium-Sulphur," Renewable and Sustainable Energy Reviews, vol. 56, pp. 1008-1021, 2016.
- [22] C. M. Birkl, M. R. Roberts, E. McTurk, P. G. Bruce, and D. A. Howey, "Degradation diagnostics for lithium ion cells," Journal of Power Sources, vol. 341, pp. 373-386, 2017.
- [23] X. Hu, F. Feng, K. Liu, L. Zhang, J. Xie, and B. Liu, "State estimation for advanced battery management: Key challenges and future trends," Renewable and Sustainable Energy Reviews, vol. 114, p. 109334, 2019.
- [24] L. Gao, S. Liu, and R. A. Dougal, "Dynamic lithium-ion battery model for system simulation," IEEE transactions on components and packaging technologies, vol. 25, no. 3, pp. 495-505, 2002.
- [25] V. Ramadesigan et al., "Modeling and simulation of lithium-ion batteries from a systems engineering perspective," Journal of The Electrochemical Society, vol. 159, no. 3, pp. R31-R45, 2012.
- [26] A. Sakti et al., "Consistency and robustness of forecasting for emerging technologies: The case of Li-ion batteries for electric vehicles," Energy Policy, vol. 106, pp. 415-426, 2017.
- [27] G. L. Plett, "Extended Kalman filtering for battery management systems of LiPB-based HEV battery packs: Part 1. Background," Journal of Power sources, vol. 134, no. 2, pp. 252-261, 2004.
- [28] D. W. Gao, C. Mi, and A. Emadi, "Modeling and simulation of electric and hybrid vehicles," Proceedings of the IEEE, vol. 95, no. 4, pp. 729-745, 2007.
- [29] B. Wu, V. Yufit, M. Marinescu, G. J. Offer, R. F. Martinez-Botas, and N. P. Brandon, "Coupled thermal–electrochemical modelling of uneven heat generation in lithium-ion battery packs," Journal of Power Sources, vol. 243, pp. 544-554, 2013.
- [30] X. Lin et al., "A lumped-parameter electro-thermal model for cylindrical batteries," Journal of Power Sources, vol. 257, pp. 1-11, 2014.
- [31] A123 Systems, "Nanophosphate® High Power Lithium Ion Cell ANR26650M1-B," ed, 2011.
- [32] C. Zhang, J. Jiang, Y. Gao, W. Zhang, Q. Liu, and X. Hu, "Charging optimization in lithium-ion batteries based on temperature rise and charge time," Applied Energy, vol. 194, pp. 569-577, 2017.
- [33] G. Liebig, V. Renaudin, R. Teodorescu, and F. Blaabjerg, "State-of-Charge Balancing Strategy for Switched Reluctance Motors with Integrated Battery Energy Storage System," IEEE Transactions on Industry Applications, vol. 56, no. 5, pp. 5524-5532, 2020.
- [34] X. Hu, C. Zou, C. Zhang, and Y. Li, "Technological developments in batteries: a survey of principal roles, types, and management needs," IEEE Power and Energy Magazine, vol. 15, no. 5, pp. 20-31, 2017.
- [35] L. H. Saw, Y. Ye, and A. A. Tay, "Integration issues of lithium-ion battery into electric vehicles battery pack," Journal of Cleaner Production, vol. 113, pp. 1032-1045, 2016.
- [36] S. Panchal, I. Dincer, M. Agelin-Chaab, R. Fraser, and M. Fowler, "Experimental and theoretical investigations of heat generation rates for a water cooled LiFePO4 battery," International Journal of Heat and Mass Transfer, vol. 101, pp. 1093-1102, 2016.
- [37] J. Yi, U. S. Kim, C. B. Shin, T. Han, and S. Park, "Three-dimensional thermal modeling of a lithium-ion battery considering the combined effects of the electrical and thermal contact resistances between current collecting tab and lead wire," Journal of the Electrochemical Society, vol. 160, no. 3, pp. A437-A443, 2013.
- [38] R. Kantharaj and A. M. Marconnet, "Heat generation and thermal transport in lithium-ion batteries: A scale-bridging perspective," Nanoscale and Microscale Thermophysical Engineering, vol. 23, no. 2, pp. 128-156, 2019.
- [39] M. Keyser et al., "Enabling fast charging–Battery thermal considerations," Journal of Power Sources, vol. 367, pp. 228-236, 2017.
- [40] G. L. Plett, "Extended Kalman filtering for battery management systems of LiPB-based HEV battery packs: Part 2. Modeling and identification," Journal of power sources, vol. 134, no. 2, pp. 262-276, 2004.
- [41] Y. Zou, X. Hu, H. Ma, and S. E. Li, "Combined state of charge and state of health estimation over lithium-ion battery cell cycle lifespan for electric vehicles," Journal of Power Sources, vol. 273, pp. 793-803, 2015.
- [42] K. T. Chau, C. C. Chan, and C. Liu, "Overview of permanent-magnet brushless drives for electric and hybrid electric vehicles," IEEE Transactions on industrial electronics, vol. 55, no. 6, pp. 2246-2257, 2008.
- [43] K.-J. Lee, K. Park, and J.-M. Kim, "Robust sensorless control for permanent magnet synchronous motor using novel speed estimation method based on augmented state observer," Energies, vol. 11, no. 11, p. 3064, 2018.
- [44] S. Li, S. Huang, X. Tao, and C. Xing, "A comparative study of FOC for PMSM based on SVPWM and SPWM," in 2019 22nd International Conference on Electrical Machines and Systems (ICEMS), 2019: IEEE, pp. 1-6.
- [45] G. Genta, "Motor vehicle dynamics," 1997.
- [46] H. Pacejka, Tire and vehicle dynamics. Elsevier, 2005.
- [47] B. Nykvist and M. Nilsson, "Rapidly falling costs of battery packs for electric vehicles," Nature climate change, vol. 5, no. 4, pp. 329-332, 2015.
- [48] T. Hofman and C. H. Dai, "Energy efficiency analysis and comparison of transmission technologies for an electric vehicle," in 2010 IEEE Vehicle Power and Propulsion Conference, 2010: IEEE, pp. 1-6.

- [49] L. Li et al., "Analysis of downshift's improvement to energy efficiency of an electric vehicle during regenerative braking," Applied Energy, vol. 176, pp. 125-137, 2016.
- [50] D. Deng, "Li-ion batteries: basics, progress, and challenges," Energy Science & Engineering, vol. 3, no. 5, pp. 385-418, 2015.
- [51] J. Jaguemont, L. Boulon, P. Venet, Y. Dubé, and A. Sari, "Lithium-ion battery aging experiments at subzero temperatures and model development for capacity fade estimation," IEEE Transactions on Vehicular Technology, vol. 65, no. 6, pp. 4328-4343, 2015.
- [52] J. Wang et al., "Degradation of lithium ion batteries employing graphite negatives and nickel-cobalt-manganese oxide+ spinel manganese oxide positives: Part 1, aging mechanisms and life estimation," Journal of Power Sources, vol. 269, pp. 937-948, 2014.
- [53] M. Ecker et al., "Development of a lifetime prediction model for lithium-ion batteries based on extended accelerated aging test data," Journal of Power Sources, vol. 215, pp. 248-257, 2012.
- [54] J. Li, A. Meintz, K. Fang, and J. Marcicki, "A multiscale computational approach for effective prognostics of lithiumion batteries," Journal of Power Sources, vol. 477, p. 228681, 2020.
- [55] J. Remmlinger, M. Buchholz, M. Meiler, P. Bernreuter, and K. Dietmayer, "State-of-health monitoring of lithium-ion batteries in electric vehicles by on-board internal resistance estimation," Journal of Power Sources, vol. 196, no. 12, pp. 5357-5363, 2011.
- [56] R. Xiong, L. Li, and J. Tian, "Towards a smarter battery management system: A critical review on battery state of health monitoring methods," Journal of Power Sources, vol. 405, pp. 18-29, 2018.
- [57] Y. Liu, B. Li, F. Luo, and Y. Peng, "Optimal charging control for lithium-ion battery packs: A distributed average tracking approach," IEEE Transactions on Industrial Informatics, vol. 16, no. 5, pp. 3430-3438, 2020.
- [58] X. Lai, Y. Zheng, and T. Sun, "A comparative study of different equivalent circuit models for estimating state-of-charge of lithium-ion batteries," Electrochimica Acta, vol. 259, pp. 566-577, 2018.
- [59] R. R. Richardson, C. R. Birkl, M. A. Osborne, and D. A. Howey, "Gaussian process regression for in situ capacity estimation of lithium-ion batteries," IEEE Transactions on Industrial Informatics, vol. 15, no. 1, pp. 127-138, 2018.
- [60] C. Unterrieder et al., "Battery state estimation using mixed Kalman/H∞, adaptive Luenberger and sliding mode observer," in 2015 IEEE Vehicle Power and Propulsion Conference (VPPC), 2015: IEEE, pp. 1-6.
- [61] T. Zhang, X. Hu, Z. Li, L. Feng, and J. Zhu, "Robust multiobjective sizing optimization of a battery pack in electric vehicles with parameter uncertainty," Journal of Energy Storage, vol. 31, p. 101643, 2020.
- [62] D. I. Stroe, M. Swierczynski, A.-I. Stroe, V. Knap, R. Teodorescu, and S. J. Andreasen, "Lithium-ion battery power degradation modelling by electrochemical impedance spectroscopy," IET Renewable Power Generation, vol. 11, no. 9, pp. 1136-1141, 2017.